ACS OMEGA

http://pubs.acs.org/journal/acsodf

Article

Role of Rare Earth Elements and Entropy on the Anatase-To-Rutile Phase Transformation of TiO_2 Thin Films Deposited by Ion Beam Sputtering

Diego L. S. Scoca, Felipe Cemin, Sara A. Bilmes, Carlos A. Figueroa, Antonio R. Zanatta, and Fernando Alvarez*

Cite This: *ACS Omega* 2020, 5, 28027−28036

Read Online

ACCESS | Metrics & More | Article Recommendations | Supporting Information

ABSTRACT: The role played by oxygen vacancies and rare earth (RE) elements in the anatase-to-rutile (A−R) phase transformation of titanium dioxide (TiO_2) is still a matter of controversy. Here, we report the A−R transformation of TiO_2 thin solid films as obtained by ion beam sputtering a RE-decorated titanium target in an oxygen-rich atmosphere. The samples correspond to undoped, single-doped (Sm, Tm, and Tb), and codoped (Sm:Tb, Sm:Tm, and Sm:Tb:Tm) TiO_2 films. In the as-prepared form, the films are amorphous and contain ∼0.5 at. % of each RE. The structural modifications of the TiO_2 films due to the RE elements and the annealing treatments in an oxygen atmosphere are described according to the experimental results provided by Raman scattering, X-ray photoelectron spectroscopy, and optical measurements. The A−R transformation depends on both the annealing temperature and the characteristics of the undoped, single-doped, and codoped TiO_2 films. As reported in the literature, the A−R transformation can be inhibited or enhanced by the presence of impurities and is mostly related to energetic contributions. The experimental results were analyzed, considering the essential and stabilizing role of the entropy of mixing in the A−R transformation due to the introduction of more and multiple quantum states originated in vacancies and impurities in the anatase phase.

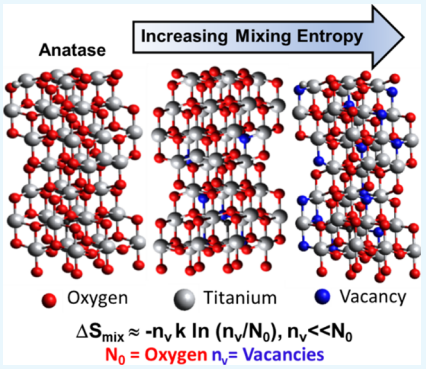

INTRODUCTION

Titanium dioxide (TiO_2) has attracted much attention in recent decades because of its applicability in areas such as pigments, optical sensors, (photo)catalysis,[1,2] ferromagnetic Fe−N-codoped TiO_2 nanotubes,[3,4] graphene-TiO_2 composites,[5] antimicrobial activity,[6] and optoelectronic devices.[7−17] Usually, TiO_2 can be found in the brookite (orthorhombic symmetry), anatase (tetragonal), and rutile (tetragonal) crystalline structures—with the last two being the most common and interesting structures for the abovementioned applications. Because rutile is the most stable phase, the anatase-to-rutile (A−R) phase transformation is an irreversible process that depends, among other factors, on the temperature, pressure, presence of impurities, grain size, synthesis processes, and post-annealing conditions.[18,19] Therefore, controlling the TiO_2 phase formation is a challenge to guarantee its final performance in many practical devices. An interesting route to manage the TiO_2 structure is by inserting small amounts of foreign species (doping), which can either inhibit or promote the development of certain phases. Doping with rare earth (RE) elements can introduce new optical properties to TiO_2. In fact, when embedded into solid matrices, trivalent RE (RE^{3+}) ions are behind many technological applications,[20−22] most of them involving efficient light emission in the ultraviolet−visible−infrared frequency range.[23−25] Moreover, by combining the electronic properties of the TiO_2 semiconductor with the RE^{3+}-related optical features, it is possible to build devices such as photon waveguides, solar cells, color displays, light-emitting diodes, and temperature sensors.[26] Finally, it is well established that doping with Sm^{3+} or Tb^{3+} improves the photocatalytic activity and stabilizes the anatase phase of TiO_2.[27]

With the aim of improving the understanding of the influence of RE impurities on the A−R transformation, this work contains a comprehensive study of undoped TiO_2 films and either single-doped (Tm, Sm, or Tb) or codoped (Sm:Tb, Sm:Tm, or Sm:Tm:Tb) thin films. In addition to the deposition and sequential thermal annealing of the films, this work comprises the examination of their composition [by X-ray photoelectron spectroscopy (XPS)], structure (by Raman scattering), and optical electronic (by UV−vis optical transmission) properties. Based on the consistent results obtained

Received: July 25, 2020
Accepted: October 9, 2020
Published: October 23, 2020

Table 1. Summary of the Compositional (XPS Data) and Structural Results (as Obtained by Raman Spectroscopy) of the Ion Beam-Sputtered TiO_2 Films[a]

		single-doped			codoped		
	undoped	Sm 0.5 at. % ±0.2	Tb 0.5 at. % ±0.2	Tm 0.5 at. % ±0.2	Sm:Tb 1 at. % ±0.4	Sm:Tm 1 at. % ±0.4	Sm:Tb:Tm 1.5 at. % ±0.6
as-dep, °C	a-TiO_2	a-TiO_2:Sm	a-TiO_2:Tb	a-TiO_2:Tm	a-TiO_2:Sm:Tb	a-TiO_2:Sm:Tm	a-TiO_2:Sm:Tb:Tm
~600	A	A	A	A	A/R	a-TiO_2:Sm:Tm	a-TiO_2:Sm:Tb:Tm
~800	A	A	A	A	A/R	R	R
~1000	A/R	A	A	A	A/R	R	R
~1170	A/R	A	A/R	A	R	R	R

[a]All of the as-deposited films are amorphous (a-TiO_2). After the first annealing stage, the anatase (A) phase is identified in single-doped films, while in codoped films (Sm + Tm- and Sm + Tb + Tm), the samples remain amorphous. Depending on the doping (element and concentration), the Raman signal shows the rutile (R) phase merging at different annealing stages.

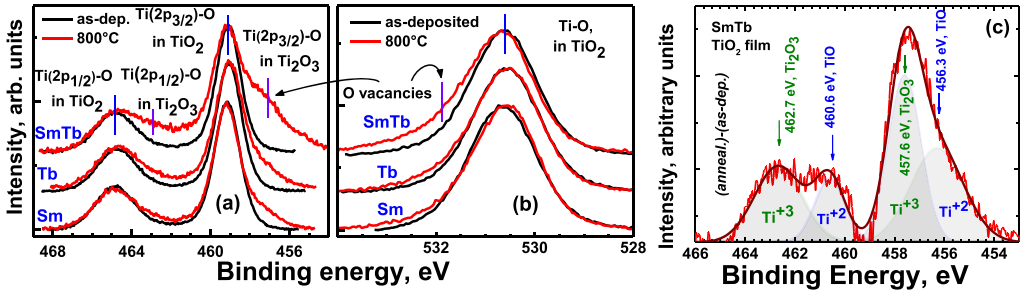

Figure 1. (a) Ti 2p; (b) O 1s electron core levels as obtained from the XPS measurements of the TiO_2 films doped with Sm, Tb, and SmTb, as-deposited and after thermal annealing at 800 °C. The presence of oxygen vacancies is indicated in the figures, denoting their susceptibility to thermal annealing treatment and doping characteristics; (c) subtraction of the SmTb-codoped TiO_2 film XPS spectrum obtained after thermal annealing from the XPS spectrum of the as-deposited sample. The deconvoluted components as well as the oxidation states are indicated.

in previous studies, the structural characteristics (*i.e.*, amorphous-crystalline nature and A−R phase proportion) of the TiO_2 films were obtained, with high precision, by Raman spectroscopy.[26,28] Grazing-incidence X-ray diffraction is also an appropriate technique to study the structure of the films; however, Raman spectroscopy is faster and essentially gives the same information.

An important section of the paper discusses how the increasing presence of oxygen vacancies in the material upon annealing is related to the increasing entropy of mixing of the system, as an attempt of understanding the A−R transformation invoking a basic thermodynamic approach. Note that the goal of the analysis, however, is to study the influence of defects on the A−R transformation and not the specific mechanism(s) of their formation. Indeed, the chemistry of the defect formation in TiO_2 is a well-established subject because of its importance in the performance of the applications mentioned above.[19] Moreover, the control of defect formation and its effect on the structure on several materials is very important, for example, in ternary uranium oxides,[29] metals,[30] and semiconductors.[31] In particular, the observed formation of the anatase or rutile phases in the TiO_2 films is consistent with the presence of RE^{3+} and RE^{2+} ions and the formation of oxygen vacancies,[19,32] as also shown in our XPS and UV−vis analyses.

The role of oxygen vacancies is studied based on the following: a perfect crystal is free of vacancies at $T = 0$ K. On the other hand, it is well known that, at higher temperatures, a real crystal contains vacancies in thermal equilibrium. The reason that it is permitted to a flawed crystal to be defective arises from a decreasing free energy ΔG due to the entropy of mixing (ΔS_{mix}) introduced by the vacancies. That is, the negative energy introduced by the $T\Delta S_{mix}$ term allows to minimize the ΔG of the system at different temperatures T.[33]

Finally, it is remarked that the role of ΔS_{mix} in the last decade has attracted much attention because of its important function in stabilizing multicomponent alloys.[34,35]

RESULTS

Surface Electronic Structure Analysis: XPS. The chemical composition of the as-deposited TiO_2 thin films and after the thermal annealing at ~1000 °C (*ex situ*) was obtained from the XPS spectra. These analyses considered the Ti 2p doublets ($2p_{3/2}$ and $2p_{1/2}$ orbitals) located at ~459 and ~464 eV, respectively, along with the following core levels: O 1s at ~531 eV, Sm 4d at ~132 eV, and Tb 4d at ~150 eV.[26,36] According to the XPS analysis, all TiO_2 films were almost stoichiometric ([Ti] ~30 ± 3 at. % and [O] ~70 ± 7 at. %) and presented the following RE concentrations: [Sm] ≈ [Tb] ≈ [Tm] ~0.5 at. % and [Sm + Tb] ~1 at. % with a ~0.5 at. % contribution of each RE. The data corresponding to SmTm- and SmTbTm-doped TiO_2 films are shown in Table 1.

Figure 1 shows the XPS spectra of a representative set of RE-doped TiO_2 films, as-deposited and after thermal annealing at 800 °C. The bands associated with the Ti 2p [Figure 1a] and O 1s [Figure 1b] core levels, along with the main titanium−oxygen bonding configurations and features associated with oxygen vacancies, are also indicated. According to Figure 1a, the Ti_2O_3-related signal increases after thermal annealing at 800 °C—as observed as shoulders at ~463 and ~457 eV.[37−39] Moreover, they are more intense in the SmTb-doped film, merging with the Ti^{3+}-related signal, denoting the presence of oxygen vacancies.[40,41] The advent of oxygen vacancies is also evident in Figure 1b, where in each case, after thermal annealing, a high-energy shoulder merges on the left of the O 1s core level.[38,40,42] In order to evince the Ti oxidation states of the SmTb-codoped TiO_2 film arising after thermal annealing,

https://dx.doi.org/10.1021/acsomega.0c03431
ACS Omega 2020, 5, 28027−28036

we subtracted the XPS spectrum obtained after thermal annealing from the XPS spectrum of the as-deposited sample. The resulting curve is shown in Figure 1c. It is remarked that oxygen vacancies are not only associated with Ti^{3+} ions but also with the presence of Ti^{2+} ions,[37−39,43] both defects contributing to increase the optical subgap absorption (see the next section). Also, in the single-doped films, these contributions are less evident (not shown).

Optical Properties: UV−vis Optical Transmission Measurements. The importance of band gap studies on TiO_2 is linked to several technological applications such as catalysis and photovoltaic devices. This is so because TiO_2 is transparent to visible light and band gap modifications are necessary to improve the subgap absorption for the cited applications. The absorption is intimately dependent on the material defects.[44,45] As noted in the introduction, the importance of the defects is one of the subjects of this paper and it has been studied by optical analysis. Therefore, the band gaps and the subgap absorption of all TiO_2 films were estimated from their respective optical absorption coefficient spectra, as obtained from the UV−vis transmission measurements.[46,47] Concerning the band structure of TiO_2, theoretical calculations have shown that the rutile and anatase phases present direct and indirect optical band gaps, respectively.[48,49] However, considering the amorphous and/or polycrystalline character of the present TiO_2 films,[50] their optical band gaps were estimated by Tauc's method.[51] Because our interest is to compare band gap variations, Tauc's method satisfies this objective. Figure 2a shows the band gaps of the TiO_2 films obtained from this method, and Figure 2b shows their evolution as a function of the annealing treatment.

For the sake of simplicity, Figure 3a_1−a_4 shows the optical absorption spectra, as-deposited and after thermal annealing at 600 and 1000 °C of selected TiO_2 films (undoped and Sm-, SmTb-, and Sm:Tm-doped). The codoped films have both a pronounced band gap shrinkage and increased sub-band gap absorption because of defects and higher doping concentration. It is remarked that in all the annealed samples, the sub-band gap absorption increases, which is in agreement with the fact that defects are created during the thermal annealing procedure.[52] The density of states is associated with the subgap absorption. Therefore, Figure 3b_1,b_2 shows the sub-band gap area *versus* annealing temperature, as obtained by integrating the low-energy region of the optical absorption curves (*e.g.*, hatched region curve in Figure 3a_3). The highest energy integrating limit was fixed at the slope intersection of the abrupt slope changes.

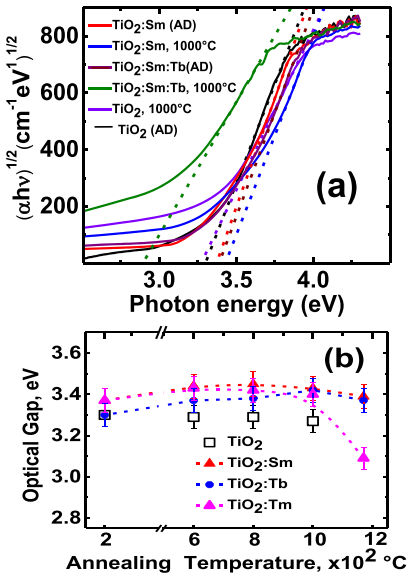

Figure 2. (a) Tauc's plots of the selected TiO_2 films (as-deposited and after thermal annealing at 1000 °C): undoped, Sm-doped, and SmTb-doped. The band gap is obtained by the intersection at the *x*-axis of the absorption edge linear fitting (dashed straight lines); (b) optical band gaps of single-doped samples as a function of thermal annealing. The dashed lines are guides for the eyes. For the sake of clarity, only the optical properties of a selected group of samples are represented in Figure 1b.

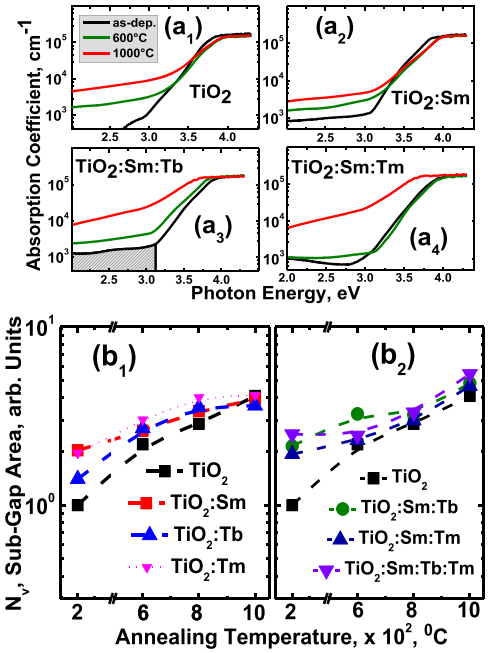

Figure 3. (a_1−a_4) Optical absorption coefficient *vs* photon energy for a select group of samples (undoped and single- and codoped), as-deposited and after thermal annealing at 600 and 1000 °C. (b_1,b_2) Normalized sub-band gap area N_v *vs* annealing temperature, as obtained by integrating the low-energy region of the absorption spectra (*e.g.*, hatched region curve a_3). The highest energy integrating limit was fixed at the slope intersection of the (abrupt) slopes changing in the absorption spectra. The dashed lines are guides for the eyes.

Structural Behavior: Raman Spectroscopy. The Raman spectroscopy results show that all the as-deposited TiO_2 films are amorphous. Moreover, depending on the doped RE element, structural changes occur at different thermal annealing temperatures (Figure 4), clearly indicating the development of the anatase (vibrational modes at ∼144, 397, 516, and 639 cm^{-1}) and/or rutile phases (∼235, 449, and 610 cm^{-1}).[53] The rutile fraction of each TiO_2 film was obtained by fitting Lorentzian curves to the anatase- and rutile-related Raman components in the 300−700 cm^{-1} range.[54] The result is illustrated in Figure 5a, which shows the Raman spectrum of the SmTb-doped TiO_2 film (after thermal annealing at 600 °C). The fraction of the rutile phase in undoped and Tb- and SmTb-doped TiO_2 films as a function of the thermal annealing temperature is presented in Figure 5b. A summary of the structural properties as a function of thermal annealing of the studied samples is provided in Table 1.

https://dx.doi.org/10.1021/acsomega.0c03431
ACS Omega 2020, 5, 28027−28036

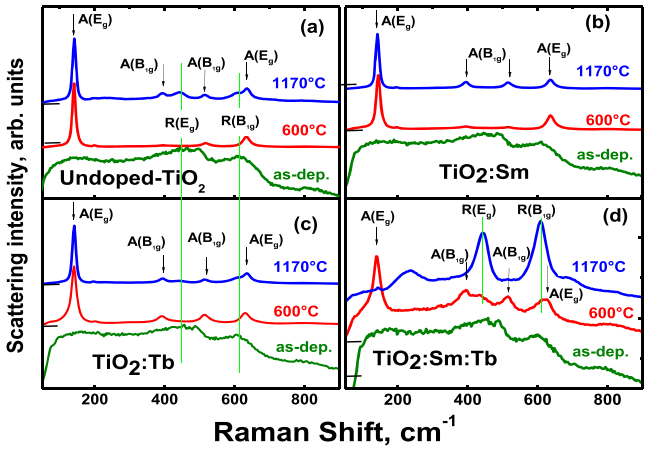

Figure 4. Raman spectra of TiO_2 films: (a) undoped, (b) Sm-, (c) Tb-, and (d) SmTb-codoped samples—as-deposited and after thermal annealing at 600 and 1170 °C. The main vibrational modes associated with the anatase (black arrows) and rutile (vertical green lines) phases of TiO_2 are indicated. For the sake of clarity, the curves were normalized and vertically shifted.

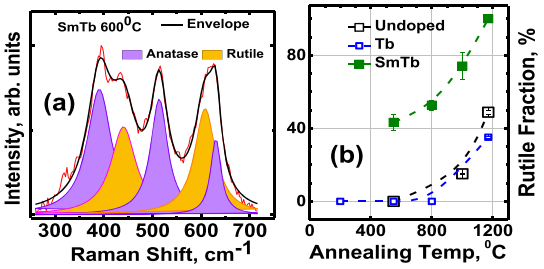

Figure 5. (a) Typical spectrum deconvolution denoting the Raman contributions due to the anatase and rutile phases of TiO_2 (SmTb-doped after thermal annealing at 600 °C). (b) Rutile fraction as a function of the annealing temperature. For the sake of clarity, only the selected samples are plotted (see Table 1): undoped and Tb- and SmTb-doped. Note that the single Tm- and Sm-doped samples are similar to a single Tb-doped sample. The dashed lines are guides for the eyes, and the error bars result from the fitting procedure.

DISCUSSION

As mentioned in the Introduction, there is a consensus in the literature that an important factor in the A−R transformation is the presence (intentional or not) of impurities in the TiO_2 host.[6,19] This transformation assumes atom diffusion, nucleation, and growth processes, with the participation of oxygen vacancies.[19,55] Regarding the doping of TiO_2 with RE elements, there are several reports showing that these species act as efficient inhibitors of the A−R transformation.[19,56−58] Hanaor and Sorrel suggest that the A−R transformation is favored by the presence of vacancies of oxygen sublattice and also show that impurities can prevent the A−R transformation.[19] Indeed, many doping elements inhibiting the A−R transformation are reported in the literature, which lead us to conclude that the limit of solubility is not reached.[19,59] The conflicting reports about the effect of impurities on either preventing or promoting the A−R transformation revealed the complexity of the phenomenon. Therefore, in the following paragraphs, we shall discuss in more detail this problem by describing a mechanism focusing on the effect of entropy in the phenomenon of the A−R transformation.

Amorphous to Anatase/Rutile Transformation. Among the various growth conditions influencing the phase transformation in amorphous TiO_2 (*e.g.*, type of substrate, deposition method, temperature, pressure, thermal treatments, and atmosphere), the grain size and thermal annealing rate are important in the A−R transformation process.[60−63] As stated by Zhang *et al.*,[64] amorphous TiO_2 is an important precursor of single-phase nanocrystalline anatase. According to these researchers, the amorphous material consists of distorted shells containing strained anatase-like structures that are important for the formation of the anatase phase. Indeed, the as-deposited nondoped and low-doped (∼0.5 at. % impurities) TiO_2 films considered in this research are amorphous, evolving to anatase as a result of the annealing treatment, provided that the temperature is maintained below ∼600−800 °C (see Table 1). Alternatively, with higher concentrations of impurities in codoped samples (∼1.0−1.5 at. %), they transform from amorphous to the anatase/rutile mixture or attain pure rutile characteristics even at lower temperatures. The latest effect could be when the concentration of impurities went beyond the solubility limit, promoting precipitation (Table 1).

A−R Transformation of Undoped TiO_2. Because of the complexity of the problem, we shall first discuss the A−R transformation of undoped TiO_2, keeping in mind that for bulk TiO_2, the rutile phase is the thermodynamically stable structure[65] and that film crystallization is prompted by annealing.[19,66] One can notice that there is enormous data dispersion for the temperature of the A−R transformation because of the rate of annealing treatments and the presence of impurities. One plausible mechanism involving the crystallization of amorphous TiO_2 relies on *topological* arguments associated with the so-called *edge-to-vertex r-ratio* linking octahedral building units. The polymorph crystalline rutile and anatase share two (2) and four (4) edges, respectively.[18] Because of the lack of long-range order in TiO_2 amorphous material submitted to the annealing process of crystallization, a *small percentage* to vertex linked ratio could be present in the precursor material. If it is so, the material evolves directly into the rutile phase upon annealing treatments. On the contrary, the anatase phase emerges when the *edge-to-vertex* linked percentage is relatively larger in the starting amorphous material.[66−68]

Thermodynamic studies of the A−R transformation involve different approaches. Taking into account that the anatase and rutile phases have the same entropy S, Chen and Mao proposed that the stability is governed by the enthalpy H and that the variation of the Gibbs free energy ΔG can be approximated by $\Delta G \approx \Delta H$.[9] In another approach, Jamieson and Olinger assumed both zero internal energy U in the A−R transformation and $\Delta G^0 \approx P\Delta V$, where ΔV is the volume variation and P is the pressure. Then, $(\Delta G^0/\Delta V)_{U,S} = P$. By substituting the ΔG^0 value reported by Navrotsky and Kleppa[69] and the molar volume variation during the transformation, the results show that negative pressures are necessary to stabilize the anatase phase. In our understating, however, the "hypothetical negative pression" mentioned by Jamieson and Olinger is a negative magnitude from $P\Delta V$ due to a difference of relative pressures and not by the presence of a negative absolute pressure.[18] Moreover, experimental results confirm that the bulk anatase phase is metastable up to ∼600−800 °C under atmospheric pressure conditions, provided that TiO_2 is pure.[19] Notably, however, none of the described

https://dx.doi.org/10.1021/acsomega.0c03431
ACS Omega 2020, 5, 28027−28036

thermodynamic and topological approaches consider the entropy effects introduced by the presence of oxygen vacancies and defects.

To understand the occurrence of the A−R transformation, we suggest that two important thermodynamic considerations should be contemplated. First, why does the A−R transformation of pure TiO_2 occur at ∼600−800 °C at atmospheric pressure? That is, why is the irreversible phase change to stable rutile hindered up to relatively high temperatures? Second, considering the experimental reports showing that this change depends on the presence of oxygen vacancies and that the rate of the A−R transformation increases exponentially with temperature, what is the role of entropy in the phase transformation?[19] With these two questions in mind, we discuss the A−R transformation of pure TiO_2 with a simple statistical model usually applied to metal alloys, where the role of entropy allows us to explain the metastability of these materials at temperatures up to $T \sim 600-800$ °C.

First, let us assume that at a fixed temperature, the anatase metastable phase is constituted, in addition to Ti atoms, by two oxygen species: vacancies and atoms in thermodynamic equilibrium. On the other hand, the temperature dependence of the density of oxygen vacancies n_v is determined in a first approximation by the Boltzmann exponential[33,70]

$$n_v = N_0 \exp(-\varepsilon_v/kT) \tag{1}$$

where ε_v is the energy necessary to create a vacancy, T is the absolute temperature, k is the Boltzmann constant, and N_0 is the number of bulk oxygen atoms in correctly coordinated sites, that is, neglecting the contribution of surface atoms (relative to the ones in the volume). In eq 1, it is assumed that the detached atoms move to the free surface of the system.[62]

Provided that the system is below the temperature of the A−R transformation, one can assume that, for a constant oxygen pressure and temperature, the system is in a thermodynamic (metastable) equilibrium, that is, vacancies and oxygen atoms are at (metastable) equilibrium. More precisely, for a fixed temperature T, the Gibbs free energy $G = U + PV - TS = H - TS$ verifies that $\Delta G = \Delta H - T\Delta S = 0$, that is, the free energy is in a local minimum (non-absolute) of the anatase metastable phase. This is similar to what occurs with diamond, which, for all purposes, is in a (metastable) equilibrium up to very high temperatures at atmospheric pressure.

During a sufficiently slow annealing (adiabatic) procedure at temperatures below the A−R transformation, TiO_2 reaches new successive metastable equilibrium states, preventing the A−R transformation. In other words, the anatase metastable phase remains "frozen" at different constant temperatures. However, as commented above, the existence of unintentional impurities and other defects can act as nucleation centers, and longer annealing times could prompt the formation of rutile crystallites, even though the quasi-equilibrium treatments are performed below ∼600−800 °C. Neglecting these effects and assuming that the anatase phase is preserved up to this critical temperature range, the variation in the Gibbs free energy for anatase is given by (assuming P and T constants) $\Delta G = \Delta U - T\Delta S$, where $\Delta V \approx 0$ is also assumed, that is, the volume does not change, which might prove that the A−R transformation does not occur. Indeed, in the experiments reported here at atmospheric pressure, a volume contraction of ∼8% arises only in the case that the A−R transformation takes place.[19] However, as the vacancies (defects) increase as a function of the annealing temperature, the entropy should be considered because the number of possible quantum microstates of the mixture also increases. Indeed, theoretical and experimental studies have shown that oxygen vacancies are formed beneath the surface of the material where the mobility of the atoms is greater than in the bulk, contributing to network rearrangement.[71] One can go further with these arguments by assuming an ideal binary solid solution constituted by N_0 and n_v, and the entropy of mixing is given by[30]

$$\Delta S_{mix} = -Nk[x_0 \ln(N_0/N) + x_v \ln(n_v/N)] \tag{2}$$

where $x_0 = N_0/N$, $x_v = n_v/N$, and $N = N_0 + n_v$. Assuming $n_v \ll N_0$, to guarantee the material's integrity

$$\Delta S_{mix} \approx -n_v k \ln\left(\frac{n_v}{N_0}\right) \tag{3}$$

Substituting n_v given by eq 1 in 3

$$\Delta S_{mix} \approx \frac{n_v \varepsilon_v}{T} \text{ or } T\Delta S_{mix} - n_v\varepsilon_v \approx 0 \tag{4}$$

The energy $n_v\varepsilon_v$ is the internal energy variation ΔU delivered to the system to create n_v vacancies,[33] that is, $\Delta U = n_v\varepsilon_v$. Therefore, $\Delta G = \Delta U - T\Delta S_{mix} \approx n_v\varepsilon_v - T\Delta S_{mix} = 0$. In conclusion, the increase of the internal energy increases the defect density, but it is compensated by the entropic negative $T\Delta S_{mix}$ energy contribution.

We remark that this type of thermodynamic approach is well known in metallic alloys, such as steel, where the increasing of the internal energy and the creation of vacancies in the system by heating the material is compensated by an increase in the entropy of mixing, which stabilizes the material at different temperatures.[30]

This effect is valid to some extent, and further increase of the internal energy ΔU can generate a larger amount of vacancies that cannot be compensated by the increasing $T\Delta S_{mix}$ and phase transition occurs. This could explain why in pure bulk TiO_2, a further increase in temperature ($T \geq 800$ °C) provokes A−R transformation.

The discussion outlined in this section suggests that entropy considerations can contribute to understanding equilibrium mixtures, such as TiO_2, at $T \neq 0$ K. We shall return to this point below. Finally, it is remarked that the phonon contribution to the total entropy of the crystal was neglected. This contribution stems from the fact that a missing atom (vacancy) decreases the constraints of its near neighbors, and thus, more local random motions are allowed, diminishing the energy ε_v (Equation 1). In other words, only ΔS_{mix} is considered because it is often larger than the phonon contribution for temperatures much lower than the melting point.[72]

A−R Transformation of RE-Doped TiO_2. In undoped TiO_2, the metastable stability of the anatase phase upon increasing the annealing temperature was explained by the compensation of the increasing ΔU (and concomitant vacancy creation) by the ΔS_{mix} increase. In doped TiO_2, the complexity of the thermodynamic problem prevents a simple analysis and only qualitative discussions and heuristic arguments can be invoked. Indeed, the presence of impurities increases the difficulty of calculating the possible combinations to estimate the entropy of mixing because a numerical method of analysis is necessary. Nevertheless, in the next subsection, we show experimental results supporting the fact that the formation of

https://dx.doi.org/10.1021/acsomega.0c03431
ACS Omega 2020, 5, 28027−28036

oxygen vacancies is independent of the impurities causing the defects.

As mentioned above, there is abundant bibliography showing that different impurities can inhibit or promote the A−R transformation.[19] In fact, single-doped samples with Sm, Tb, or Tm are examples of the former, *that is*, the anatase phase is stable up to higher annealing temperatures (Figure 5b and Table 1). These RE elements seem to be good inhibitors of the A−R transformation, in agreement with the comprehensive study by Hishita *et al.*[32] At first glance, a larger number of impurities suggests that the increasing entropy of mixing could favor the stabilization of the metastable phase because the $-T\Delta S_{mix}$ term could contribute to minimizing the Gibbs free energy. Nevertheless, there are other effects that could invalidate this simple argument. For instance, increasing doping concentration could promote the A−R transformation by the formation of rutile nucleation centers. In fact, our results show that codoping at RE concentration ≥1 at. % destabilizes the anatase phase at lower annealing temperatures (Figure 5b and Table 1) because of the aggregation of defects[2] and, probably, kinetics effects.

The incorporation of impurities (promoting or preventing the A−R transformation) is expected to depend also on the creation of oxygen vacancies.[19] Additionally, stemming from structural constraints, the inclusion of dopants (in substitutional or interstitial sites) also influences the transformation. Finally, previous reports on the subject show that both the atomic radius and valence of the dopants seem to promote nucleation and thus the transformation.[35] From a thermodynamic point of view, even considering an ideal solid solution, the presence of four species (Ti, RE, O, and vacancies) makes the calculation of the Gibbs function a serious problem. In addition, the entropy of mixing assumes that the solid solution components can occupy the sites randomly, a condition that is not realistic because preferential bonding of the atoms acts during the formation of the material.[19,35] Moreover, the inclusion of a dopant in the RE^{+3} state of oxidation increases the entropy of the system, and the assumption of an ideal entropy of mixing of two species is a rough approximation. We understand that all these questions are difficult to answer satisfactorily at the present stage of the results obtained in this work. However, the experimental findings show that single-doped samples, independently on the REs considered (Sm, Tb, and Tb), show a similar increase in the density of subgap defects (oxygen vacancies) as a function of the annealing temperature (Figure 3b$_1$). Therefore, it is suggested that ΔS_{mix} is the most important factor stabilizing the material at higher annealing temperatures. Moreover, as we shall show in the next section, the activation energy associated with the generation of vacancies is the same, within the experimental error, for all the single-doped samples, supporting the argument that the type of defects created by the impurities (Sm, Tb, and Tm) behaves similarly (Figure 6a). We suggest that this argument is valid, provided that the RE atoms are occupying substitutional or interstitial sites forming a solid solution, a situation most likely limited by the impurity concentration, as discussed in the beginning of this section.[73]

To summarize, one can conclude that the inclusion of single-doped RE elements will increase the entropy of mixing, stabilizing the anatase phase. In fact, an approach to the complex problem of the equilibrium phases of multicomponent alloys was addressed by several authors (please see ref 35 and

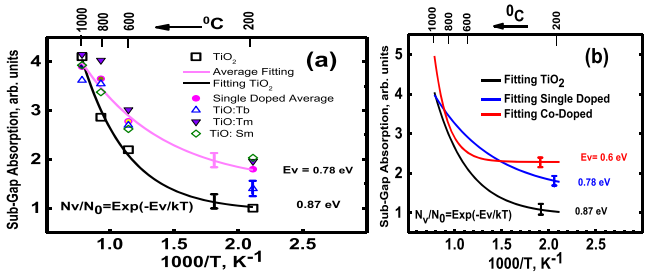

Figure 6. (a) Sub-band gap absorption areas obtained from Figure 3b$_1$ *vs* $10^3/T$ (annealing temperature). The black solid lines (square symbols) correspond to the exponential fitting for the undoped TiO_2 films. The magenta solid line (rhombus symbols) is an exponential fitting corresponding to the average sub-band gap absorption areas of all the single-doped samples. For comparison purposes, the sub-band gap absorption curves *vs* 10^3/T are compiled in (b), including the average curve of the codoped samples displayed in Figure 3b$_2$. For the sake of clarity, the symbols of the experimental data are suppressed. The value of the activation energies E_v of the exponential fittings are indicated. Note that the symbol E_v is used to distinguish from the previous one (ε_v) to make it clear that the former is an experimental and specific value of the energy necessary to create an individual vacancy for doped samples.

references therein). A short discussion of these basic ideas is outlined in the Supporting Information.

Sub-Band Gap Absorption and Density of Defects. The sub-band gap absorption evolution of the undoped TiO_2 films is a consequence of defect creation prompted by thermal treatment. As noted above, Figure 1a−c shows the merging of the bands associated with Ti^{3+} and Ti^{2+} defects associated with Ti_2O_3 and TiO structures.[38−40] Additionally, Figure 3b$_1$,b$_2$ shows a monotonical increase in sub-band gap absorption due to the defect states for both single- and codoped samples as the annealing treatment advances.

Regarding the creation of oxygen vacancies, there is consensus in the literature that they are easier to create compared to Ti interstitial.[52,74] This effect means that most of the states associated with sub-band gap absorption N_v represented in Figure 3 can be ascribed to oxygen vacancies, and one can equate n_v to N_v, that is, $n_v \approx N_v$. Figure 6 shows that in pure and single-doped TiO_2 films, the sub-band gap densities of defects merge altogether at the higher studied annealing temperature. Within the experimental error, the single-doped films show a similar behavior over the entire range of annealing temperatures. As discussed in the previous section, this finding suggests that there is no specificity in the creation of sub-band gap defects associated with the RE dopants. With these considerations in mind, we fitted the experimental sub-band gap absorption data by using the expression $N_v = N_0 \exp(-E_v/kT)$ of the TiO_2 films, undoped (E_v = 0.87 eV), single-doped (average E_v = 0.78 eV), and codoped (E_v = 0.60 eV) [Figure 6a,b]. E_v is associated with the energy necessary to create an individual vacancy for doped samples. Note that the symbol E_v is used to distinguish it from the previous ε_v to make it clear that the latter is an experimental and specific energy value to form a vacancy for doped samples. To estimate N_0, stoichiometric TiO_2 was assumed to have a density of 3.894 g cm^{-3} (Figure 7).[19] Moreover, in the frame of the present study, the defect (vacancies) involved in the entropy is estimated by the subgap absorption spectra; however, other strategies can be used, for example, those reported by Zhou *et al.*[4]

https://dx.doi.org/10.1021/acsomega.0c03431
ACS Omega 2020, 5, 28027−28036

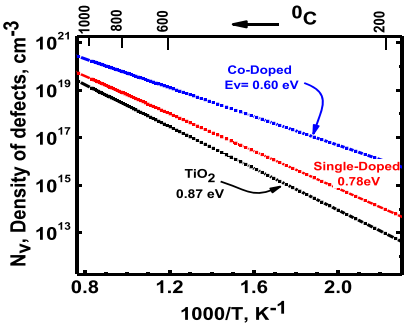

Figure 7. Theoretical density of vacancies assuming the activation energies obtained from the fittings in Figure 6b. The number N_0 was estimated assuming stoichiometric TiO_2 and a density of 3.894 g cm^{-3}.[10]

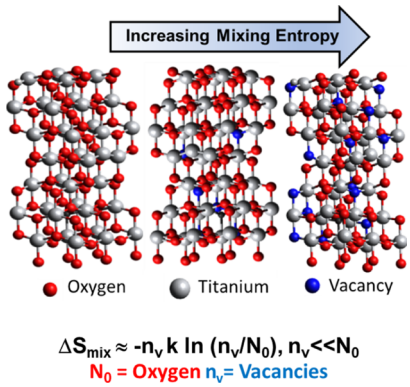

Figure 8. Artistic representation of the anatase-rutile transformation. The stoichiometric TiO_2 structure is assumed in the left part of the picture. Increasing temperature prompt an increase of vacancies (blue symbols). Consequently, an increasing entropy of mixing also occurs.

From these results, one can draw the following findings. First, up to ∼1100 °C, the concentration of oxygen vacancies is larger in single-doped films than in undoped TiO_2. This result implies that the entropy term ($T\Delta S_{mix}$) is larger in the former samples than in the undoped samples, compensating for the increasing enthalpy of the lattice incremented by the annealing treatment. Consequently, in the single-doped films, the anatase phase is stabilized even at temperatures higher than the range normally found for the A−R transformation of undoped TiO_2 (Figure 5). Second, the rapid growth of defects in all the studied films (at the higher annealing temperatures) leads to a larger increase of density of the defects. This merging suggests that at higher annealing treatments, the internal energy ΔU [Equation 2] is so high that the $T\Delta S_{mix}$ energy associated to entropy is not enough to compensate the increase of ΔU, prompting the A−R transformation. Moreover, for a large density of vacancies, the contribution of the $P\Delta V$ term is an important driving force for the A−R transformation because the rutile density is ∼8% higher than the anatase density.[6] For codoped samples, Figure 7 shows a high density of defects (vacancies), even for relatively low annealing temperatures, explaining why the rutile phase occurs at lower annealing temperatures [Figure 5b]. In fact, codoped samples contain twice the concentration of RE elements, and nucleation centers of the rutile phase are probably prompting the phase transformation.

Finally, a qualitative argument about the A−R transformation is presented with the help of a graphical picture (Figure 8). Assuming constant temperature and $T \neq 0$ K, the system is in a minimum of the Gibbs function. The annealing treatment increases the internal energy ΔU, pushing the system out of the (metastable) equilibrium. However, the number of vacancies n_v also increases because of the increase of the temperature. Therefore, an increasing entropy of mixing ΔS_{mix} is expected and, to some extent, it could compensate the increase of the internal energy of the system, ΔU, bringing the system to a new local equilibrium.

SUMMARY AND CONCLUSIONS

TiO_2 films (undoped as well as doped with Sm, Tm, Tb, SmTm, SmTb, and SmTmTb) were deposited by ion beam sputtering of a Ti target properly decorated with Sm, Tm, and/or Tb elements. In the as-deposited samples, Raman and XPS measurements indicate that all the films are amorphous and approximately stoichiometric ([Ti] ∼ 30 at. % and [O] ∼ 70 at. %). The single-doped films contain ∼0.5 at. % and the codoped films contain ∼1−1.5 at. %. The anatase-to-rutile transformation was studied by sequential thermally annealing the films under a flow of oxygen at slightly higher atmospheric pressure in the 600−1170 °C temperature range. In addition to the compositional (XPS analysis) and structural (Raman) characterization, the optical properties of the films were investigated by UV−vis transmission spectroscopy. According to the experimental results, the thermal treatments increase the sub-band gap absorption of the material because of the creation of oxygen vacancies. The importance of these defects regarding the phase transformation was discussed, focusing on the thermodynamic role of the entropy of mixing by considering vacancies and oxygen atoms. In the pure TiO_2 films, it is proposed that the increasing density of oxygen vacancies on annealing treatment is compensated, to some extent, by the increasing of the entropy of mixing, preventing the A−R transformation. This thermodynamic approach is well known in metallic alloys, such as steel, where the increasing in the internal energy and the creation of vacancies by heating the material are compensated by the increasing energy of mixing ($T\Delta S$), which stabilizes the material at relatively higher temperatures. For higher annealing temperatures, the exponential growth of oxygen vacancies favors the A−R transformation. On the other hand, the transformation was prevented up to ∼1000 °C in the Sm- and Tb-doped films. The inclusion of several RE^{3+} and RE^{2+} ions in the TiO_2 structure increases the complexity of the calculation of the entropy of mixing, and only qualitative arguments are suggested. Indeed, increasing the possible arrangements of vacancies associated with oxygen bonded either to the RE^{3+}, RE^{2+}, or Ti^{4+} species also increases the entropy of mixing. This increasing helps to stabilize the doped films up to higher temperatures compared with the one observed in pure TiO_2. However, further increasing the RE doping over ∼1.0−1.5 at. % prompts the A−R transformation. Precise calculations using numerical models such as those used in the so-called multi-principal element alloys could bring more quantitative conclusions.

EXPERIMENTAL DETAILS

TiO_2 films (undoped, single-doped, and codoped with Sm, Tb, and Tm) were deposited on both crystalline Si and fused silica substrates by argon ion beam sputtering of a Ti (99.999%) target decorated with RE (99.9%) pieces.[30] The concentration

https://dx.doi.org/10.1021/acsomega.0c03431
ACS Omega 2020, 5, 28027−28036

of each element in the film can be controlled by properly adjusting the exposed area of each doping material on the target mosaic assembly, that is, by means of the sputtering target design. The typical deposition conditions were as follows: 2×10^{-6} mbar (base pressure), 5×10^{-4} mbar (O_2 atmosphere during deposition), ∼200 °C (substrate temperature), and 1.5 keV and 13 mA cm^{-2} (Ar^+ ion beam energy and current density). Under these conditions, the TiO_2 films were macroscopically homogeneous with a thickness of ∼300 nm, as obtained by atomic force microscopy (Vecco Innova).

After deposition, the films were investigated by *in situ* XPS measurements (1486.6 eV Al Kα line with an ∼0.85 eV energy resolution[75]), and the data were analyzed following standard procedures involving spectra background removal (Shirley method[76]) and relative chemical composition analysis (by adopting the sensitive factors of Wagner *et al.*[77]). In the experimental setup, the sputtering deposition chamber (at 10^{-6} Pa base pressure) is connected to the XPS analysis chamber (at 10^{-7} Pa) through a transference chamber (at 10^{-6} Pa). Therefore, the as-deposited samples were transferred to the XPS analysis chamber immediately after deposition, without being exposed to air. Subsequently, the films were *ex situ* thermally annealed under an oxygen atmosphere at 600, 800, 1000, and 1170 °C. The treatments were cumulative, 30 min long, and carried out at an oxygen pressure slightly above the atmospheric pressure. Because the films were exposed to ambient conditions after the thermal annealing treatments, mild surface cleaning was performed (∼100 eV Ar^+ for 30 s) before the XPS measurements. To avoid differences stemming from the cleaning procedure to the greatest extent, the procedure was performed under equivalent conditions for all the studied samples. All films, as-deposited and after each thermal annealing step, were further investigated by Raman scattering (488.0 nm photon excitation) and UV−vis (∼300−700 nm wavelength range) optical transmission measurements. Likewise, the photoluminescence of the films was investigated, and the main results can be found elsewhere.[26,36]

■ ASSOCIATED CONTENT

Supporting Information

The Supporting Information is available free of charge at https://pubs.acs.org/doi/10.1021/acsomega.0c03431.

Entropy calculations (PDF)

■ AUTHOR INFORMATION

Corresponding Author

Fernando Alvarez − *Instituto de Física Gleb Wataghin, Universidade Estadual de Campinas (UNICAMP), Campinas 13083-970, Brazil;* orcid.org/0000-0002-9393-1298; Email: alvarez@ifi.unicamp.br

Authors

Diego L. S. Scoca − *Instituto de Física Gleb Wataghin, Universidade Estadual de Campinas (UNICAMP), Campinas 13083-970, Brazil;* orcid.org/0000-0002-8632-2136

Felipe Cemin − *Instituto de Física Gleb Wataghin, Universidade Estadual de Campinas (UNICAMP), Campinas 13083-970, Brazil;* orcid.org/0000-0002-8971-2113

Sara A. Bilmes − *Universidad de Buenos Aires, Facultad de Ciencias Exactas y Naturales, Ciudad de Buenos Aires C1428EGA, Argentina; CONICET - Universidad de Buenos Aires. Instituto de Química de Materiales, Medio Ambiente y Energía (INQUIMAE), Ciudad de Buenos Aires C1428EHA, Argentina*

Carlos A. Figueroa − *Programa de Pós-Graduação em Engenharia e Ciência dos Materiais, Universidade de Caxias do Sul (UCS), Caxias do Sul 95070-560, Brazil;* orcid.org/0000-0002-9473-1626

Antonio R. Zanatta − *Instituto de Física de São Carlos, Universidade de São Paulo (USP), São Carlos 13566-590, Brazil*

Complete contact information is available at: https://pubs.acs.org/10.1021/acsomega.0c03431

Author Contributions

The manuscript was written through contributions of all authors.

Notes

The authors declare no competing financial interest.

■ ACKNOWLEDGMENTS

This work was financially supported by the Brazilian agencies FAPESP (projects 2012/10127-5 and 2019/18460-4) and FAPERGS (project 19/2551-0002288-3). Partial support of CONICET (PIP 2017-2019 GI-11220170100289CO) and UBACyT (20020170200298BA). F.C. is a FAPESP fellow, project 2018/24461-0. D.S., A.R.Z., C.A.F., and F.A. are CNPq fellows. This work is part of the PhD Thesis of D.S. The authors are indebted to C. Piacenti for his technical support. The authors acknowledge "Universidade Estadual de Campinas" (UNICAMP) for APC funding.

■ REFERENCES

(1) Nowotny, M. K.; Sheppard, L. R.; Bak, T.; Nowotny, J. Defect Chemistry of Titanium Dioxide. Application of Defect Engineering in Processing of TiO2-Based Photocatalysts. *J. Phys. Chem. C* **2008**, *112*, 5275−5300.

(2) Nowotny, J. *Oxide Semiconductors for Solar Energy Conversion Titanium Dioxide*, 1st ed.; Lee, S., Ed.; CRC Press: Boca Raton, FL 33487-2742, 2012.

(3) Zhou, Z.; Wang, H.; Yang, Z. Intrinsic defect-mediated magnetism in Fe-N codoped TiO 2. *J. Alloys Compd.* **2016**, *657*, 372−378.

(4) Zhou, Z.; Yang, X.; Wang, H.; Zou, Z.; Guo, J. Electronic and Magnetic Properties Studies on Mn and Oxygen Vacancies Codoped Anatase TiO2. *Adv. Condens. Matter Phys.* **2016**, *2016*, 1−7.

(5) Zhang, N.; Yang, M.-Q.; Liu, S.; Sun, Y.; Xu, Y.-J. Waltzing with the Versatile Platform of Graphene to Synthesize Composite Photocatalysts. *Chem. Rev.* **2015**, *115*, 10307−10377.

(6) Onna, D.; Fuentes, K. M.; Spedalieri, C.; Perullini, M.; Marchi, M. C.; Alvarez, F.; Candal, R. J.; Bilmes, S. A. Wettability, Photoactivity, and Antimicrobial Activity of Glazed Ceramic Tiles Coated with Titania Films Containing Tungsten. *ACS Omega* **2018**, *3*, 17629−17636.

(7) Regazzoni, A. E.; Mandelbaum, P.; Matsuyoshi, M.; Schiller, S.; Bilmes, S. A.; Blesa, M. A. Adsorption and Photooxidation of Salicylic Acid on Titanium Dioxide: A Surface Complexation Description. *Langmuir* **1998**, *14*, 868.

(8) Angelomé, P. C.; Andrini, L.; Calvo, M. E.; Requejo, F. G.; Bilmes, S. A.; Soler-Illia, G. J. A. A. Mesoporous Anatase TiO2 Films: Use of Ti K XANES for the Quantification of the Nanocrystalline Character and Substrate Effects in the Photocatalysis Behavior. *J. Phys. Chem. C* **2007**, *111*, 10886.

(9) Chen, X.; Mao, S. S. Titanium Dioxide Nanomaterials: Synthesis, Properties, Modifications, and Applications. *Chem. Rev.* **2007**, *107*, 2891−2959.

(10) Liu, H.; Yu, L.; Chen, W.; Li, Y. The Progress of Nanocrystals Doped with Rare Earth Ions. *J. Nanomater.* **2012**, *2012*, 1−9.
(11) Bingham, S.; Daoud, W. A. Recent advances in making nano-sized TiO2visible-light active through rare-earth metal doping. *J. Mater. Chem.* **2011**, *21*, 2041−2050.
(12) Pereira, A. L. J.; Lisboa Filho, P. N.; Acuña, J.; Brandt, I. S.; Pasa, A. A.; Zanatta, A. R.; Vilcarromero, J.; Beltrán, A.; Dias da Silva, J. H. Enhancement of optical absorption by modulation of the oxygen flow of TiO2 films deposited by reactive sputtering. *J. Appl. Phys.* **2012**, *111*, 113513.
(13) Hao, C.; Liao, Y.; Wu, Y.; An, Y.; Lin, J.; Gu, Z.; Jiang, M.; Hu, S.; Wang, X. RuO2-loaded TiO2-MXene as a high performance photocatalyst for nitrogen fixation. *J. Phys. Chem. Solids* **2020**, *136*, 109141.
(14) Chu, Z.; Qiu, L.; Chen, Y.; Zhuang, Z.; Du, P.; Xiong, J. TiO2-Loaded Carbon Fiber: Microwave Hydrothermal Synthesis and Photocatalytic Activity under UV Light Irradiation. *J. Phys. Chem. Solids* **2020**, *136*, 109138.
(15) Xie, Q.; Fu, Z.; Wei, X.; Li, X.; Yue, W.; Kang, J.; Zhu, L.; Wang, C.; Meng, J. Effect of Substrate Bias Current on Structure and Properties of CrNx Films Deposited by Plasma Enhanced Magnetron Sputtering. *Surf. Coating. Technol.* **2019**, *365*, 134−142.
(16) Cassaignon, S.; Colbeau-Justin, C.; Durupthy, O. Titanium Dioxide in Photocatalysis. *Nanomaterials: A Danger or a Promise?*; Springer London: London, 2013; pp 153−188.
(17) Pan, X.; Yang, M.-Q.; Fu, X.; Zhang, N.; Xu, Y.-J. Defective TiO2 with Oxygen Vacancies: Synthesis, Properties and Photocatalytic Applications. *Nanoscale* **2013**, *5*, 3601.
(18) Jamieson, J. C.; Olinger, B. Pressure-Temperature Studies of Anatase, Brookite, Rutile and TiO2(II): A Discussion. *Am. Mineral.* **1969**, *54*, 1477−1481.
(19) Hanaor, D. A. H.; Sorrell, C. C. Review of the Anatase to Rutile Phase Transformation. *J. Mater. Sci.* **2011**, *46*, 855−874.
(20) Yu, H.-F.; Chen, L.-H. P/Si-TiO2 Transparent Films with High Anatase Stability and Photocatalytic Activity. *J. Phys. Chem. Solids* **2011**, *72*, 269−275.
(21) Kenyon, A. Recent Developments in Rare-Earth Doped Materials for Optoelectronics. *Prog. Quant. Electron.* **2002**, *26*, 225−284.
(22) Steckl, A. J.; Park, J. H.; Zavada, J. M. Prospects for Rare Earth Doped GaN Lasers on Si. *Mater. Today* **2007**, *10*, 20−27.
(23) Zanatta, A. R.; Khan, A.; Kordesch, M. E. Red−Green−Blue Light Emission and Energy Transfer Processes in Amorphous SiN Films Doped with Sm and Tb. *J. Phys. Condens. Matter* **2007**, *19*, 436230.
(24) Zanatta, A. R.; Nunes, L. A. O. Green Photoluminescence from Er-Containing Amorphous SiN Thin Films. *Appl. Phys. Lett.* **1998**, *72*, 3127−3129.
(25) Polman, A. Erbium as a Probe of Everything? *Phys. B Condens. Matter* **2001**, *300*, 78−90.
(26) Zanatta, A. R.; Scoca, D.; Alvarez, F. A Suitable (Wide-Range + Linear) Temperature Sensor Based on Tm^{3+}Ions. *Sci. Rep.* **2017**, *7*, 14113.
(27) Saif, M.; Abdel-Mottaleb, M. S. A. Titanium Dioxide Nanomaterial Doped with Trivalent Lanthanide Ions of Tb, Eu and Sm: Preparation, Characterization and Potential Applications. *Inorg. Chim. Acta.* **2007**, *360*, 2863−2874.
(28) Scoca, D.; Morales, M.; Merlo, R.; Alvarez, F.; Zanatta, A. R. Photoluminescence and Compositional-Structural Properties of Ion-Beam Sputter Deposited Er-Doped TiOfilms: Their Potential as a Temperature Sensor. *J. Appl. Phys.* **2015**, *117* (). DOI: DOI: 10.1063/1.4921809.
(29) Murphy, G. L.; Wang, C.-H.; Zhang, Z.; Kowalski, P. M.; Beridze, G.; Avdeev, M.; Muransky, O.; Brand, H. E. A.; Gu, Q.-F.; Kennedy, B. J. Controlling Oxygen Defect Formation and Its Effect on Reversible Symmetry Lowering and Disorder-to-Order Phase Transformations in Nonstoichiometric Ternary Uranium Oxides. *Inorg. Chem.* **2019**, *58*, 6143−6154.
(30) Haasen, P.; Mordike, B. L. *Physical Metallurgy*; Cambridge University Press, 1996.
(31) Fox, M. *Optical Properties of Solids*, 2nd ed.; Oxford University Press (Verlag): Oxford, 2010.
(32) Hishita, S.; Mutoh, I.; Koumoto, K.; Yanagida, H. Inhibition Mechanism of the Anatase-Rutile Phase Transformation by Rare Earth Oxides. *Ceram. Int.* **1983**, *9*, 61−67.
(33) Blakemore, J. S. *Solid State Physics*, 2nd ed.; ; Cambridge University Press: Cambridge, 1985.
(34) Miracle, D. B.; Senkov, O. N. A Critical Review of High Entropy Alloys and Related Concepts. *Acta Mater.* **2017**, *122*, 448−511.
(35) Cemin, F.; Jimenez, M. J. M.; Leidens, L. M.; Figueroa, C. A.; Alvarez, F. A Thermodynamic Study on Phase Formation and Thermal Stability of AlSiTaTiZr High-Entropy Alloy Thin Films. *J. Alloys Compd.* **2020**, *838*, 155580.
(36) Zanatta, A. R.; Scoca, D.; Alvarez, F. Influence of the Anatase and Rutile Phases on the Luminescent Properties of Rare-Earth-Doped TiO2 Films. *J. Alloys Compd.* **2019**, *780*, 491−497.
(37) Chan, C.-M.; Trigwell, S.; Duerig, T. Oxidation of an NiTi Alloy. *Surf. Interface Anal.* **1990**, *15*, 349−354.
(38) Oja Acik, I.; Kiisk, V.; Krunks, M.; Sildos, I.; Junolainen, A.; Danilson, M.; Mere, A.; Mikli, V. Characterisation of Samarium and Nitrogen Co-Doped TiO2 Films Prepared by Chemical Spray Pyrolysis. *Appl. Surf. Sci.* **2012**, *261*, 735−741.
(39) Marchi, M. C.; Bilmes, S. A.; Ribeiro, C. T. M.; Ochoa, E. A.; Kleinke, M.; Alvarez, F. A Comprehensive Study of the Influence of the Stoichiometry on the Physical Properties of TiOx Films Prepared by Ion Beam Deposition. *J. Appl. Phys.* **2010**, *108*, 064912.
(40) Bharti, B.; Kumar, S.; Lee, H.-N.; Kumar, R. Formation of Oxygen Vacancies and Ti3+ State in TiO2 Thin Film and Enhanced Optical Properties by Air Plasma Treatment. *Sci. Rep.* **2016**, *6*, 32355.
(41) Pan, J. M.; Maschhoff, B. L.; Diebold, U.; Madey, T. E. Interaction of Water, Oxygen, and Hydrogen with TiO 2 (110) Surfaces Having Different Defect Densities. *J. Vac. Sci. Technol., A* **1992**, *10*, 2470−2476.
(42) Lin, Y. B.; Yang, Y. M.; Zhuang, B.; Huang, S. L.; Wu, L. P.; Huang, Z. G.; Zhang, F. M.; Du, Y. W. Ferromagnetism of Co-Doped TiO 2 Films Prepared by Plasma Enhanced Chemical Vapour Deposition (PECVD) Method. *J. Phys. D: Appl. Phys.* **2008**, *41*, 195007.
(43) Bilmes, S. A.; Mandelbaum, P.; Alvarez, F.; Victoria, N. M. Surface and Electronic Structure of Titanium Dioxide Photocatalysts. *J. Phys. Chem. B* **2000**, *104*, 9851−9858.
(44) Naldoni, A.; Altomare, M.; Zoppellaro, G.; Liu, N.; Kment, Š.; Zbořil, R.; Schmuki, P. Photocatalysis with Reduced TiO2: From Black TiO2 to Cocatalyst-Free Hydrogen Production. *ACS Catal.* **2019**, *9*, 345−364.
(45) Ullattil, S. G.; Narendranath, S. B.; Pillai, S. C.; Periyat, P. Black TiO2 Nanomaterials: A Review of Recent Advances. *Chem. Eng. J.* **2018**, *343*, 708−736.
(46) Swanepoel, R. Determination of the Thickness and Optical Constants of Amorphous Silicon. *J. Phys. E.* **1983**, *16*, 1214−1222.
(47) Zanatta, A. R. Effect of Thermal Annealing Treatments on the Optical Properties of Rare-Earth-Doped AlN Films. *J. Phys. D: Appl. Phys.* **2009**, *42*, 025109.
(48) Asahi, R.; Taga, Y.; Mannstadt, W.; Freeman, A. J. Electronic and optical properties of anataseTiO2. *Phys. Rev. B: Condens. Matter Mater. Phys.* **2000**, *61*, 7459−7465.
(49) Pascual, J.; Camassel, J.; Mathieu, H. Fine structure in the intrinsic absorption edge of TiO2. *Phys. Rev. B: Condens. Matter Mater. Phys.* **1978**, *18*, 5606−5614.
(50) Scoca, D.; Morales, M.; Merlo, R.; Alvarez, F.; Zanatta, A. R. Photoluminescence and compositional-structural properties of ion-beam sputter deposited Er-doped TiO2−xNx films: Their potential as a temperature sensor. *J. Appl. Phys.* **2015**, *117*, 205304.
(51) Tauc, J. Optical Properties and Electronic Structure of Amorphous Ge and Si. *Mater. Res. Bull.* **1968**, *3*, 37−46.

https://dx.doi.org/10.1021/acsomega.0c03431
ACS Omega 2020, 5, 28027−28036

(52) Morgan, B. J.; Watson, G. W. Intrinsic n-type Defect Formation in TiO2: A Comparison of Rutile and Anatase from GGA+U Calculations. *J. Phys. Chem. C* **2010**, *114*, 2321−2328.
(53) Tompsett, G. A.; Bowmaker, G. A.; Cooney, R. P.; Metson, J. B.; Rodgers, K. A.; Seakins, J. M. The Raman Spectrum of Brookite, TiO2 (Pbca, Z = 8). *J. Raman Spectrosc.* **1995**, *26*, 57−62.
(54) Zanatta, A. R. A fast-reliable methodology to estimate the concentration of rutile or anatase phases of TiO2. *AIP Adv.* **2017**, *7*, 075201.
(55) Chen, C. H.; Kelder, E. M.; Schoonman, J. Electrostatic Sol-Spray Deposition (ESSD) and Characterisation of Nanostructured TiO 2 Thin Films. *Thin Solid Films* **1999**, *342*, 35−41.
(56) Forissier, S.; Roussel, H.; Chaudouet, P.; Pereira, A.; Deschanvres, J.-L.; Moine, B. Thulium and Ytterbium-Doped Titanium Oxide Thin Films Deposited by Ultrasonic Spray Pyrolysis. *J. Therm. Spray Technol.* **2012**, *21*, 1263−1268.
(57) Borlaf, M.; Colomer, M. T.; Moreno, R.; Ortiz, A. L. Rare Earth-Doped TiO2 Nanocrystalline Thin Films: Preparation and Thermal Stability. *J. Eur. Ceram. Soc.* **2014**, *34*, 4457−4462.
(58) Jia, C. W.; Xie, E. Q.; Zhao, J. G.; Sun, Z. W.; Peng, A. H. Visible and Near-Infrared Photoluminescences of Europium-Doped Titania Film. *J. Appl. Phys.* **2006**, *100*, 023529.
(59) Janes, R. Structural and Spectroscopic Studies of Iron (III) Doped Titania Powders Prepared by Sol-Gel Synthesis and Hydrothermal Processing. *Dyes Pigm.* **2004**, *62*, 199−212.
(60) Zhang, H.; Banfield, J. F. Understanding Polymorphic Phase Transformation Behavior during Growth of Nanocrystalline Aggregates: Insights from TiO2. *J. Phys. Chem. B* **2000**, *104*, 3481−3487.
(61) Barnard, A. S.; Zapol, P. Effects of Particle Morphology and Surface Hydrogenation on the Phase Stability of TiO2. *Phys. Rev. B: Condens. Matter Mater. Phys.* **2004**, *70*, 235403.
(62) Reidy, D. J.; Holmes, J. D.; Morris, M. A. The Critical Size Mechanism for the Anatase to Rutile Transformation in TiO2 and Doped-TiO2. *J. Eur. Ceram. Soc.* **2006**, *26*, 1527−1534.
(63) Rao, A.; Pundir, V. S.; Tiwari, A.; Padarthi, Y.; Rao, N. V. M.; Aich, S.; Roy, B. Investigating the Effect of Dopant Type and Concentration on TiO 2 Powder Microstructure via Rietveld Analysis. *J. Phys. Chem. Solids* **2018**, *113*, 164−176.
(64) Zhang, H.; Chen, B.; Banfield, J. F.; Waychunas, G. A. Atomic Structure of Nanometer-Sized Amorphous TiO2. *Phys. Rev. B: Condens. Matter Mater. Phys.* **2008**, *78*, 214106.
(65) SHANNON, R. D.; PASK, J. A. Kinetics of the Anatase-Rutile Transformation. *J. Am. Ceram. Soc.* **1965**, *48*, 391−398.
(66) Jing, F.; Harako, S.; Komuro, S.; Zhao, X. Luminescence Properties of Sm 3+ -Doped TiO 2 Thin Films Prepared by Laser Ablation. *J. Phys. D: Appl. Phys.* **2009**, *42*, 085109.
(67) Petkov, V.; Holzhüter, G.; Tröge, U.; Gerber, T.; Himmel, B. Atomic-Scale Structure of Amorphous TiO2 by Electron, X-Ray Diffraction and Reverse Monte Carlo Simulations. *J. Non-Cryst. Solids* **1998**, *231*, 17−30.
(68) Mavračić, J.; Mocanu, F. C.; Deringer, V. L.; Csányi, G.; Elliott, S. R. Similarity Between Amorphous and Crystalline Phases: The Case of TiO 2. *J. Phys. Chem. Lett.* **2018**, *9*, 2985−2990.
(69) Navrotsky, A.; Kleppa, O. J. Enthalpy of the Anatase-Rutile Transformation. *J. Am. Ceram. Soc.* **1967**, *50*, 626.
(70) Tabor, D. *Gases, Liquids and Solids and Other States of Matter*, 3rd ed.; Cambridge University Press: Cambridge, 1991; Vol. *29*.
(71) He, Y.; Dulub, O.; Cheng, H.; Selloni, A.; Diebold, U. Evidence for the Predominance of Subsurface Defects on Reduced Anatase TiO2(101). *Phys. Rev. Lett.* **2009**, *102*, 106105.
(72) Archroft, N. W.; Mermin, N. D. *Solid State Physics*; Saunders College: PA, 1976.
(73) Burns, A.; Hayes, G.; Li, W.; Hirvonen, J.; Demaree, J. D.; Shah, S. I. Neodymium Ion Dopant Effects on the Phase Transformation in Sol−Gel Derived Titania Nanostructures. *Mater. Sci. Eng. B* **2004**, *111*, 150−155.
(74) Zhao, H.; Pan, F.; Li, Y. A Review on the Effects of TiO2 Surface Point Defects on CO2 Photoreduction with H2O. *J. Mater.* **2017**, *3*, 17−32.
(75) Hammer, P.; Victoria, N. M.; Alvarez, F. Electronic Structure of Hydrogenated Carbon Nitride Films. *J. Vac. Sci. Technol., A* **1998**, *16*, 2941−2949.
(76) Briggs, D.; Seah, M. P. *Pratical Surface Analysis*, 2nd ed.; Briggs, D., Seah, M. P., Eds.; John Wiley & Sons, Ltd: Chichester, UK, 1990; Vol. *1*.
(77) Wagner, C. D.; Davis, L. E.; Zeller, M. V.; Taylor, J. A.; Raymond, R. H.; Gale, L. H. Empirical Atomic Sensitivity Factors for Quantitative Analysis by Electron Spectroscopy for Chemical Analysis. *Surf. Interface Anal.* **1981**, *3*, 211−225.

https://dx.doi.org/10.1021/acsomega.0c03431
ACS Omega 2020, 5, 28027−28036